Zero-mean circular Bessel statistics and Anderson localization

Jason A. Newman, Yulu Chen, and Kevin J. Webb
School of Electrical and Computer Engineering, Purdue University, 465 Northwestern Avenue, West Lafayette, Indiana 47907-1285, USA
(Received 20 May 2013; published 18 August 2014)

We demonstrate that a circular Bessel density function describes the electromagnetic field statistics in the Anderson localization regime using example numerical terahertz field data in strongly scattering media. This density function for localized fields provides a measure that allows identification and description in a manner akin to the Gaussian density function for weakly interacting scatterers, the mathematical framework to date for statistical optics. Our theory provides a framework for improved understanding of wave propagation in random media, random scattering media characterization, and imaging in and through randomly scattering media.

DOI: 10.1103/PhysRevE.90.022119 PACS number(s): 05.40.−a, 42.25.Dd, 41.20.Jb

I. INTRODUCTION

Zero-mean circular Gaussian statistics are ubiquitously assumed for electromagnetic fields in statistical optics [1]. The validity of this model hinges on the field being made up of a multitude of independent random phasors and weakly interacting scatterers. For example, polarized thermal light has circular complex Gaussian statistics because it contains a large number of independent contributions from each atom in the source. Coherent light can also produce Gaussian statistics after multiple scattering events, as would occur with transmission through certain random scattering media, including, but not limited to, diffusers, particle suspensions, and tissue [2]. Zero-mean circular Gaussian field statistics have been verified experimentally in optically thick random scattering media with weakly interacting scatterers, where the mean free path length, a measure of the mean distance between scattering events, is much larger than the wavelength and long-range correlation effects are negligible [3,4]. In this regime, all of the scattered fields in a random phasor sum description of the field at a point in space can be assumed to be statistically independent.

The statistics of a randomly scattered electromagnetic field can be non-Gaussian, or equivalently, the intensity density function can deviate from negative exponential, when there are a limited number of contributing phasors or when there are correlations between different phasors [5]. The probability density functions for the total transmission and angle-dependent transmission coefficient have been obtained using Feynman diagrams [6,7] and random matrix theory [8]. Instead of studying the effects of interference on wave transport, another line of work focused on the properties of the number of contributing random phasors, which led to a family of K-distributions [9,10]. Such distributions were found to be excellent models for various situations where the intensity statistics are not negative exponential, such as microwave radiation reflected by rough sea surfaces [9], transmission through turbulent atmosphere [11–13], and randomly corrugated waveguides [14].

Despite prior work on the deviation of intensity statistics from negative exponential, an analytical density function has not been achieved that can describe the field statistics when they are not zero-mean circular Gaussian. Inspired by previous work on the K-distribution (modified Bessel function of the second kind) [9,15,16], we derive an analytical density function for the real and imaginary parts of the field, assuming only circularity, which is satisfied in media having a sufficiently large number of random scatterers. The resulting circular density function uses a Bessel function description, and is referred to as a circular Bessel density function. The circular Bessel density function contains a degree of freedom that makes it effective in describing the numerical field statistics obtained from strong scatter, including the Anderson localization regime [17]. In this paper, we demonstrate that analytic intensity and field density functions based on a circular Bessel function field description are in excellent agreement with numerical data in these strongly scattering regimes.

II. THEORY

The K-distribution applies to situations where the field is the resultant sum of a randomly varying number of random phasors, N. Its derivation is based on the underlying fluctuation in N, where N is modeled by the negative binomial probability mass function as [15]

$$p(N) = \binom{N+\alpha-1}{N} \frac{[\langle N\rangle/\alpha]^N}{[1+\langle N\rangle/\alpha]^{N+\alpha}}. \tag{1}$$

The parameter α governs the shape of Eq. (1). When $\alpha \gg 1$, it is centered around its mean value, $\langle N\rangle$. Thus, for sufficiently large $\langle N\rangle$, any density function derived from Eq. (1) will approach Gaussian statistics. When $\alpha \ll 1$, $p(N)$ is peaked at $N = 0$ and then decreases with increasing N, which is the case for localization. This versatility in differing numbers of contributing phasors, N, makes Eq. (1) applicable to a variety of scattering regimes.

If the contributing random phasors are independent and circular, the characteristic function for the total field amplitude (A), $\psi_A(\omega)$, is the product of the characteristic functions of the amplitudes of the N contributing phasors, $\psi_A(\omega) = J_0^N(a\omega)$, where J_0 is the zeroth order Bessel function of first kind and a is the magnitude of each contributing random phasor [2]. After averaging $\psi_A(\omega)$ over N using Eq. (1) [15],

$$\langle\psi_A(\omega)\rangle_N = \left(1+\frac{\omega^2\langle A^2\rangle}{4\alpha}\right)^{-\alpha}, \quad \langle N\rangle \to \infty. \tag{2}$$

The density function for A is the inverse zeroth-order Hankel transform of Eq. (2), which in turn leads to the K-distribution for the normalized intensity after a change of variables

 ©2014 American Physical Society

($I = A^2$) and normalization ($\hat{I} = I/\langle I \rangle$), giving [9,16]

$$p(\hat{I}) = \frac{2\alpha}{\Gamma(\alpha)}(\alpha\hat{I})^{(\alpha-1)/2}K_{\alpha-1}(2\sqrt{\alpha\hat{I}}), \tag{3}$$

where Γ is the Gamma function, K denotes the modified Bessel function of the second kind, and α is a parameter that is obtained from the variance of $\hat{I}$, such that [16]

$$\sigma_{\hat{I}}^2 = 1 + 2/\alpha. \tag{4}$$

We now derive the probability density functions for the field from Eq. (2). Let ϕ_R and ϕ_I denote the real and imaginary parts of the field, respectively, so the field amplitude is $A = \sqrt{\phi_R^2 + \phi_I^2}$. Assuming that the phase of each random phasor contributing to the total field is uniformly distributed over 2π, the resultant total field will be circular [2]. Then, the characteristic functions for ϕ_R and ϕ_I will be equal to that of the amplitude A [15], given in Eq. (2), and $p(\phi_R)$ and $p(\phi_I)$ can be obtained by an inverse Fourier transform as

$$p(\phi_{R,I}) = \frac{1}{2\pi}\int_{-\infty}^{\infty}\langle\psi_A(\omega)\rangle_N e^{-i\omega\phi_{R,I}}d\omega \tag{5}$$

$$= \frac{2}{\Gamma(\alpha)}\sqrt{\frac{\alpha}{\pi\langle A^2\rangle}}\left(\sqrt{\frac{\alpha\phi_{R,I}^2}{\langle A^2\rangle}}\right)^{\alpha-0.5} \times K_{\alpha-0.5}\left(2\sqrt{\frac{\alpha\phi_{R,I}^2}{\langle A^2\rangle}}\right). \tag{6}$$

We define the normalized real/imaginary part of the field as $\hat{\phi}_{R,I} \equiv \phi_{R,I}/\sqrt{\langle A^2\rangle}$. Because $\hat{\phi}_{R,I} \equiv \phi_{R,I}/\sqrt{\langle A^2\rangle}$ is monotonic and invertible, the probability density function for $\hat{\phi}_{R,I}$ can be obtained via a change of variables using Eq. (6), giving

$$p(\hat{\phi}_{R,I}) = \frac{2}{\sqrt{\pi}\Gamma(\alpha)}\alpha^{(\alpha+0.5)/2}\left(\hat{\phi}_{R,I}^2\right)^{(\alpha-0.5)/2}K_{\alpha-0.5}\left(2\sqrt{\alpha\hat{\phi}_{R,I}^2}\right). \tag{7}$$

We call Eq. (7) the circular Bessel density function. It is a counterpart to the well-known zero-mean circular Gaussian density function, and is suitable under circumstances where the central limit theorem does not hold. With this analytical density function for field secured, we proceed to investigate its validity in describing localized fields using numerical simulations.

III. RESULTS

The two-dimensional simulation geometry we considered, shown in Fig. 1, was an 8 mm long by 2 mm wide region of lithium niobate, $LiNbO_3$ (LN), with randomly distributed 50 μm diameter dielectric-filled holes. The left and right boundaries were perfectly matched layers (PML), to absorb the scattered waves, and the top and bottom boundaries were perfect electric conductors (PECs). The boundary on the left was the input plane and that on the right was the output plane. In the simulations, a transverse magnetic 0.75 THz plane wave, having an effective wavelength of 62 μm in LN with a dielectric constant of 41.7, with $\mathbf{H}$ in the $\hat{\mathbf{z}}$-direction, was incident from the left (hence, propagating in the $\hat{\mathbf{x}}$-direction). Circular holes were distributed throughout the LN region using

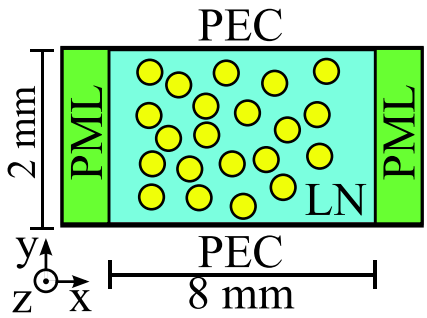

FIG. 1. (Color online) The random medium simulation geometry (not to scale) was composed of randomly distributed 50 μm diameter cylindrical holes in an 8 mm long by 2 mm wide LN region ($\epsilon_r = 41.7$): PML—perfectly matched layer; PEC—perfect electric conductor. A 0.75 THz plane wave with $\mathbf{H}$ in the $\hat{\mathbf{z}}$-direction was incident from the left.

a Gaussian density function with a mean x-spacing of $\langle x\rangle$ and a mean y-spacing of $\langle y\rangle$, and variances of σ_x^2 and σ_y^2, respectively. By varying the variance of the Gaussian hole distribution, the holes can be distributed quasiperiodically or highly randomly, as in the cases presented here. The holes were filled with various dielectrics, with dielectric constants ranging from 1 to 20, where smaller values provide stronger scatter. Due to the large contrast in the dielectric constants of LN and free space, this disordered waveguide geometry has been shown to be an excellent platform to study Anderson localization [18]. Numerical solutions were obtained using finite element method simulations (COMSOL Multiphysics). We investigated two hole distributions, both with a mean fill fraction of 0.42, $\langle x\rangle = 67\,\mu$m and $\langle y\rangle = 69\,\mu$m, and $\langle x\rangle = 78\,\mu$m and $\langle y\rangle = 60\,\mu$m, corresponding to low and high transmission for the periodic cases, respectively.

We first demonstrate localization of THz waves by analyzing the total transmitted power and intensity statistics at the output plane. The power transmitted through the random medium, T, is the integral of the Poynting vector over the plane of the detector. Let $\hat{T} = T/\langle T\rangle$ denote the normalized power transmission, where $\langle T\rangle$ is the ensemble average of T. The characteristic function of $\hat{T}$ was originally derived assuming weak scatter, under general assumptions of flux conservation and time invariance [7,8]. The probability density function of $\hat{T}$, written as the inverse Laplace transform of its characteristic function, has been shown to be [7]

$$p(\hat{T}) = \int_{-i\infty}^{i\infty}\frac{1}{2\pi i}e^{\xi\hat{T} - g\ln^2\left(\sqrt{1+\xi/g}+\sqrt{\xi/g}\right)}d\xi, \tag{8}$$

where g is the dimensionless conductance that is related to the variance of $\hat{T}$ by $\sigma_{\hat{T}}^2 = 2/(3g)$ [7,8]. A typical indicator of localization is a dimensionless conductance less than 1 [19,20], a measure of the variance of the transmission statistics. It was later shown experimentally that Eq. (8) can also be applicable in the localization regime, for both electromagnetic [20–23] and acoustic [24] waves.

From our simulation results, we obtained an estimate of g from the variance of $\hat{T}$. We compared $p(\hat{T})$ obtained from our numerical data with Eq. (8), using the estimated g and a numerical integration. We did this for holes with

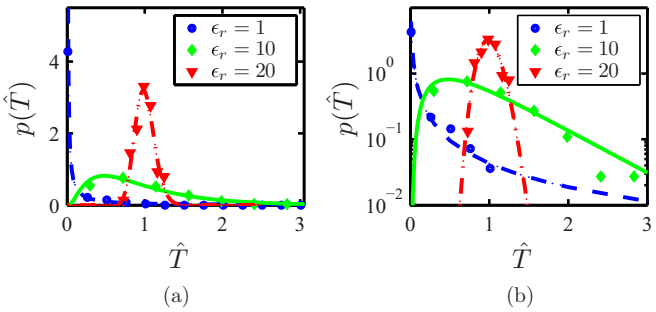

FIG. 2. (Color online) Probability density function of normalized total transmission power, $p(\hat{T})$, from numerical data (symbols) and Eq. (8) (curves) on linear (a) and semi-log (b) scales. The randomly located 50 μm diameter holes in LN ($\epsilon_r = 41.7$) had dielectric constants of 20, 10, and 1, and a fill fraction of 0.42. The hole Gaussian density function had $\langle x \rangle = 67$ μm, $\langle y \rangle = 69\,\mu$m and $\sigma_{x,y} = 7$ μm. As the hole dielectric constant decreases (increasing scatter), g decreases as well.

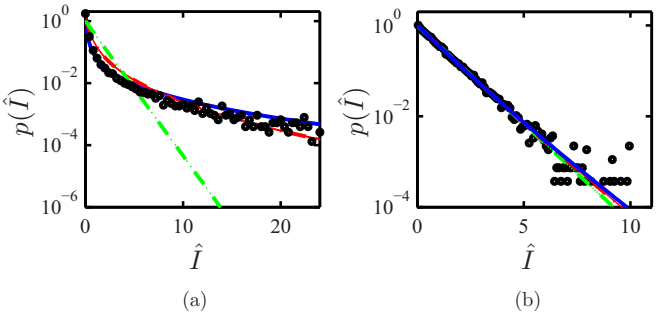

FIG. 3. (Color online) Probability density function for the normalized intensity, $\hat{I}$: negative exponential (green); theoretical result from Eq. (9) (red); K-distribution (3) (blue); numerical data (black dots). The scatterers were 50 μm diameter dielectric holes in LN, where (a) $\epsilon_r = 1$ with $g = 0.32$ and $\alpha = 0.12$, and (b) $\epsilon_r = 20$ with $g = 42$ and $\alpha = 37$. In both figures, the Gaussian-distributed holes had $\langle x \rangle = 78\,\mu$m, $\langle y \rangle = 60$ μm, and $\sigma_{x,y} = 7$ μm.

three distinct dielectric constants (ϵ_r), 1, 10, and 20, with the results shown in Fig. 2 [23]. As the dielectric constant increases, it approaches the dielectric constant of the LN background, 41.7, reducing the effective scattering strength. For each dielectric constant, the statistical data was formed from the numerical field data from 90 randomly generated hole distributions. Figure 2 shows how $p(\hat{T})$ evolves as g transitions from 42.02 (red) to 1.26 (green) to 0.02 (blue), corresponding to a transition from diffusive transport to localization with increasing strength of scatter. In the diffusive regime there are many "conducting channels" in the random medium, all contributing to the total transmission. Thus, $p(\hat{T})$ is Gaussian as a result of the central limit theorem with weaker scatter (large hole dielectric constant). As localization is approached (with smaller hole dielectric constant), the number of "conducting channels" diminishes, leading to a larger variance in $p(\hat{T})$. These characteristics of $p(\hat{T})$ are all clearly observed in Fig. 2. In the case of free space holes ($\epsilon_r = 1$), $g = 0.02$ indicates the localization regime. Note that our numerical results fit the theoretical model of Eq. (8) well in all three cases, from weak through strong scatter.

We provide a rough estimate of the localization length, $\xi \sim N\ell_s$, where N is the number of propagating modes in our geometry and ℓ_s is the scattering mean free path [20,25,26]. We assume that the random medium can be homogenized such that the geometry can be represented as a waveguide filled with a medium with an effective dielectric constant determined by Maxwell-Garnett mixing theory [27,28]. Thus, the number of modes is equal to $N = 2w/\lambda_e$, where w is the width of the waveguide (2 mm) and λ_e is the effective wavelength in the homogenized medium. For $\epsilon_r = 1, 10,$ and 20, we find that N is equal to 45, 51, and 56, respectively. The scattering mean free path is given by $\ell_s = 1/(\rho\sigma_s)$, where ρ is the density of scatterers and σ_s is the scattering cross section of a single scatterer. After obtaining the scattering cross section from a numerical simulation of the scattered field for a single scatterer, we find the scattering mean free path, ℓ_s, to be 31.7 μm, 39.7 μm, and 91.6 μm for $\epsilon_r = 1, 10,$ and 20, respectively. With both N and ℓ_s calculated, the localization length is be found to be 1.4 mm, 2.0 mm, and 5.1 mm, when ϵ_r is equal to 1, 10, and 20, respectively. The calculation of the dimensionless conductance, the plot of the probability density function of the normalized total transmission, the estimate of the scattering mean free path, and the localization length all serve as important indicators of localization and allow us to establish that LN with randomly placed free space holes can localize THz waves.

We proceed to investigate the intensity probability density function, $p(\hat{I})$, at the output plane, where $\hat{I}$ is the intensity, the $\hat{\mathbf{x}}$-component of the Poynting vector normalized by its ensemble average. As long as the nth moment of the normalized intensity and total transmission are related by $\langle \hat{I}^n \rangle = n! \langle \hat{T}^n \rangle$ for all positive integers n, $p(\hat{I})$ can be obtained from $p(\hat{T})$ by [7]

$$p(\hat{I}) = \int_0^\infty \frac{1}{\hat{T}} e^{-\hat{I}/\hat{T}}\, p(\hat{T}) d\hat{T}, \tag{9}$$

where $p(\hat{I}|\hat{T}) = \hat{T}^{-1} \exp(-\hat{I}/\hat{T})$ is the conditional density for $\hat{I}$, given $\hat{T}$, arrived at by virtue of the moment dependence between $\hat{I}$ and $\hat{T}$, and Bayes' rule has been used.

We plot numerical $p(\hat{I})$ data at the output plane in Fig. 3 for the localization [Fig. 3(a)] and diffusive [Fig. 3(b)] regimes. Density functions obtained from numerical results are fitted to Eqs. (3) and (9). The negative exponential density function is also drawn for comparison.

For the case of strong scatter in Fig. 3(a), we observe that both Eqs. (3) and (9) fit our numerical data well, while the negative exponential density function decays much faster. This is the first observation that the K-distribution, given by Eq. (3), can model intensity statistics of Anderson localized waves. In this randomly scattering medium, the number of random phasors that contribute to the total field at a certain position within the random medium is itself random. The number of contributing phasors vanish at positions outside of localization regions, where the field is evanescent, and the number becomes nonzero when the position is within a localization region. These localized regions include concatenated or spatially overlapping localized modes, known as necklace states, that can transmit energy through the random medium [29]. The K-distribution (3) fits the data well because Eq. (1) is an effective model for

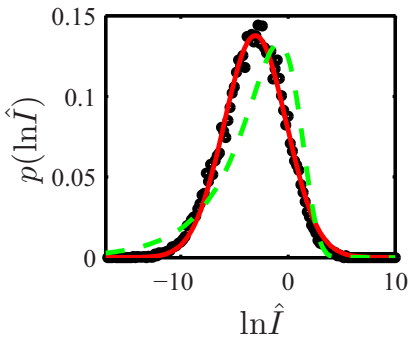

FIG. 4. (Color online) Probability density function for the natural logarithm of normalized intensity, $\ln\hat{I}$: fit to Eq. (10) with $\alpha = 0.267$ (green dashed); fit to Gaussian with mean $\mu = -3.05$ and variance $\sigma^2 = 8.37$ (red); numerical data (black dots). The numerical data are the same as in Fig. 3.

the number of random phasors that contribute to the field in the strong scatter case. Similarly, in randomly corrugated waveguides having weak scatter and a small number of contributing random phasors, it was found that the output plane field magnitude statistics could be described using the K-distribution [14].

For the case of weak scatter in Fig. 3(b), all three models fit the data well, indicating, as expected, a negative exponential probability density function for intensity. Equation (3) fits because it approaches a negative exponential density function for $\alpha \gg 1$, while Eq. (9) fits because $p(\hat{T})$ is Gaussian, with a mean of unity and small variance (approximately a Dirac delta function) in the diffusive regime. Then, $p(\hat{T})$ sifts out $\exp(-\hat{I})$ in Eq. (9), making the density function for $\hat{I}$ negative exponential.

The distribution for the logarithm of the normalized intensity in the localization regime has been predicted to be log-normal [26,30,31]. From Eq. (3), we can do a change of variables and obtain the K-distribution for $\ln\hat{I}$ as

$$p(\ln\hat{I}) = e^{\ln\hat{I}}\frac{2\alpha}{\Gamma(\alpha)}(\alpha e^{\ln\hat{I}})^{(\alpha-1)/2}K_{\alpha-1}(2\sqrt{\alpha e^{\ln\hat{I}}}). \quad (10)$$

In Fig. 4, we plot the numerical distribution of the natural logarithm of the normalized intensity data and compare it with both Eq. (10) and the Gaussian density function for $\ln\hat{I}$. The log scale provides an expanded view for normalized intensities less than one, which in Fig. 3 represents a small portion of the overall plot. The excellent agreement between the data and Gaussian fit provides additional evidence for Anderson localization. On this scale, the K-distribution also fits the data reasonably well. The random phasor sum model leading to the K-distribution for intensity allows the derivation of an analytic form for the field density function which, until now, has not been achieved. The similarity and difference between Eq. (10) and the Gaussian density function can be analyzed by studying the asymptotic forms of the modified Bessel function of second kind, $K_\nu(z)$,

$$K_\nu(z) \sim \frac{1}{2}\Gamma(\nu)\left(\frac{z}{2}\right)^{-\nu}, \quad z \to 0, \quad (11)$$

$$K_\nu(z) \sim \sqrt{\frac{\pi}{2z}}e^{-z}, \quad z \to \infty. \quad (12)$$

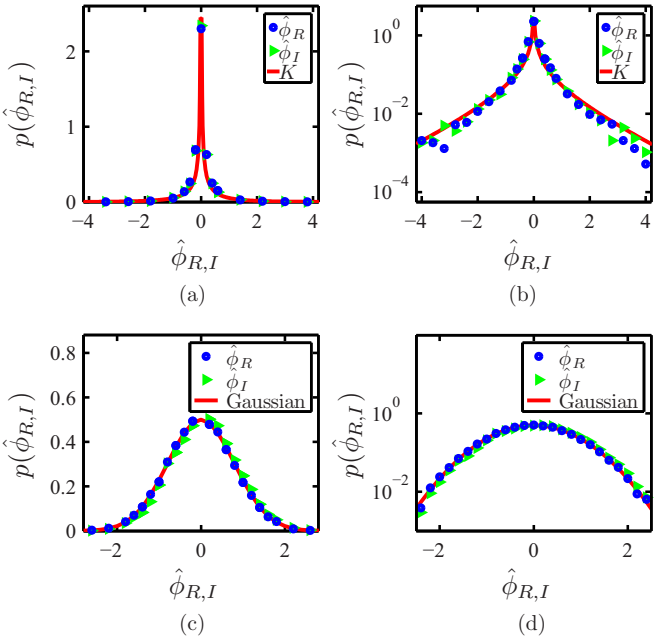

FIG. 5. (Color online) Magnetic field statistics at the output plane, on both linear and semi-log scales for clarity: (a) and (b) are for strong scatter ($\epsilon_r = 1$), where the theoretical line is calculated using Eq. (7); (c) and (d) show the weak scatter case ($\epsilon_r = 20$), with the red line being the fit to a Gaussian density function. The numerical data are the same as in Fig. 3.

Substituting Eqs. (11) and (12) into Eq. (10), we obtain

$$p(\ln\hat{I}) \sim e^{\ln\hat{I}}, \quad \hat{I} \to 0, \quad (13)$$

$$p(\ln\hat{I}) \sim e^{-e^{(\ln\hat{I})/2}}, \quad \hat{I} \to \infty. \quad (14)$$

In Eqs. (13) and (14) we only retain the term that dominates the asymptotic behavior of $p(\ln\hat{I})$. We observe from Eq. (13) that $p(\ln\hat{I})$ grows as $\exp(\ln\hat{I})$ as $\ln\hat{I}$ increases from negative infinity. This growth is slower than the form of any Gaussian density function. When $\ln\hat{I}$ approaches infinity, Eq. (14) indicates that $p(\ln\hat{I})$ decays as $\exp\{-\exp[(\ln\hat{I})/2]\}$, which is faster than any Gaussian decay. Figure 4 clearly shows these features.

Using magnetic field data at the output plane, we obtained the $p(\hat{\phi}_{R,I})$ results in Fig. 5, given on both linear and semi-log scales for clarity. Figures 5(a) and 5(b) show the localized case and Figs. 5(c) and 5(d) that for Gaussian fields and weak scatter. We can see that Eq. (7) is an excellent model for the data, making it the first analytical expression to describe the probability density function of the real and imaginary parts of fields in the localization regime.

Consider now the field statistics inside the random medium for both the diffusive and localization regimes. Referring to Fig. 1, numerical field data from the $x = 2$, 4, 6, and 8 mm planes inside the random medium resulted in the probability density functions in Fig. 6. We show only the real part of the field for clarity, the imaginary density function is the same. We find identical normalized field statistics at different depths inside the random medium, even in the case of localization.

The circular Bessel density function, Eq. (7), has been written in terms of normalized field. However, it has one free

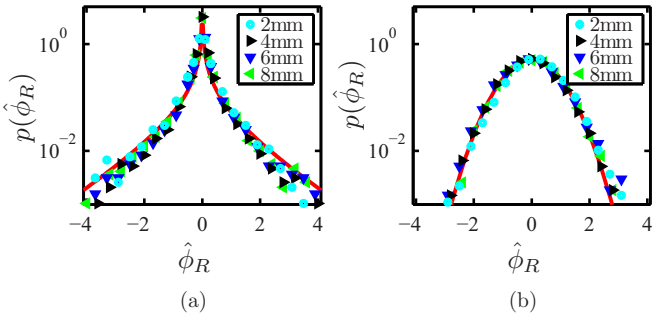

FIG. 6. (Color online) Statistics of the real part of the magnetic field taken at different depths inside the random medium: (a) strong scatter ($\epsilon_r = 1$); (b) weak scatter ($\epsilon_r = 20$). The red line shows the theoretical prediction using Eq. (7). The numerical field data are the same as that used to generate the results in Fig. 3.

variable, α, that can be traced back to Eq. (1). It is exactly the different shapes of Eq. (1) for different α that gives Eqs. (3) and (7) their versatility to model wave statistics under all scattering conditions, with only the minimal assumption of circularity. In Fig. 6(a), the invariance of the normalized field statistics as a function of depth is attributed to the contribution of necklace states to the variance (and α) in the localization regime.

All field densities in Fig. 6(b) are identical because of the normalization. We know that for zero-mean circular Gaussian statistics, $p(\phi_{R,I}) = \exp(-\phi_{R,I}^2/2\sigma^2)/\sqrt{2\pi\sigma^2}$, and the amplitude is Rayleigh distributed and given by $p(A = \sqrt{\phi_R^2 + \phi_I^2}) = A\exp[-A^2/(2\sigma^2)]/\sigma^2$ [2]. Given that $\langle A\rangle = \sqrt{\sigma^2\pi/2}$, we can eliminate σ^2 in $p(\phi_{R,I})$ by using $\hat{\phi}_{R,I} = \phi_{R,I}/\langle A\rangle$ as the new random variable, and obtain $p(\hat{\phi}_{R,I}) = 0.5\exp(-\pi\hat{\phi}_{R,I}^2/4)$. Thus, as long as the fields are zero-mean circular Gaussian, the real and imaginary parts of the field can always be normalized so that they have a probability density function that is independent of position, assuming fully developed statistics. Notice that the maximum value of the density function in Fig. 5(c), located at $\hat{\phi}_{R,I} = 0$, is exactly 0.5.

IV. CONCLUSION

The fundamental equations of physics, such as Maxwell's equations and the Schrödinger equation, use a field or wave function solution that forms the basis for the intensity or probability. Their solutions are typically represented using phasors. Our work contributes to the random phasor sum model by predicting the field density function when the number of contributing random phasors is finite. This holds not only for photon scattering in a variety of random media, but should also hold for electrons and other particles scattering in random potentials.

We have shown that the numerical field statistics in the localization regime can be well described by the circular Bessel density function. The basis of the circular Bessel density function is the random variation in the number of contributing phasors in the total field, which in turn is tied to the physical picture of Anderson localization. Although the log-normal distribution appears to be a more precise model for intensity in the localization regime, the K-distribution and the circular Bessel density function, obtained from a modified random phasor sum model, are statistical descriptions that unveil the intrinsic connection between intensity and field, thus far unavailable with the log-normal description. The discovery of the circular Bessel density function for fields builds a theoretical foundation for experiments that directly measure field [18,32]. This density function may also be a basis for the development of a moment theorem analogous to that developed for Gaussian statistics [33], which will facilitate the intensity-based characterization of random media, and imaging through and within random media. The parameter α in the circular Bessel density function is related to the scintillation index (σ_I^2), which has recently been shown to describe a fundamental length scale of waves in random media [34]. Thus, the field density function we derived may also bridge the gap between field statistics and the formation of freak waves in weakly scattering random media. Having an analytical density function that works in a variety of scattering regimes may also prove interesting in the study of random lasers [35], for example, in the design of highly directional random lasers [36].

ACKNOWLEDGMENTS

We acknowledge support from the National Science Foundation (NSF) under Grant Nos. 1028610-ECCS and 1128632-ECCS.

[1] J. W. Goodman, *Statistical Optics* (Wiley, New York, 2000).
[2] J. W. Goodman, *Speckle Phenomena in Optics: Theory and Applications* (Roberts & Co, Greenwood Village, CO, 2007).
[3] M. A. Webster, T. D. Gerke, K. J. Webb, and A. M. Weiner, Opt. Lett. **29**, 1491 (2004).
[4] T. D. Gerke, M. A. Webster, A. M. Weiner, and K. J. Webb, J. Opt. Soc. Am. A **22**, 2691 (2005).
[5] N. Shnerb and M. Kaveh, Phys. Rev. B **43**, 1279 (1991).
[6] E. Kogan, M. Kaveh, R. Baumgartner, and R. Berkovits, Phys. Rev. B **48**, 9404 (1993).
[7] E. Kogan and M. Kaveh, Phys. Rev. B **52**, R3813 (1995).
[8] T. M. Nieuwenhuizen and M. C. W. van Rossum, Phys. Rev. Lett. **74**, 2674 (1995).
[9] E. Jakeman and P. N. Pusey, IEEE Trans. Ant. Propag. **24**, 806 (1976).
[10] L. C. Andrews and R. L. Phillips, J. Opt. Soc. Am. A **3**, 1912 (1986).
[11] V. S. R. Gudimetla and J. F. Holmes, J. Opt. Soc. Am. **72**, 1213 (1982).
[12] J. H. Churnside and R. J. Hill, J. Opt. Soc. Am. A **4**, 727 (1987).
[13] L. C. Andrews, R. L. Phillips, and B. K. Shivamoggi, Appl. Opt. **27**, 2150 (1988).

[14] A. García-Martín, J. J. Sáenz, and M. Nieto-Vesperinas, Phys. Rev. Lett. **84**, 3578 (2000).
[15] E. Jakeman and P. N. Pusey, Phys. Rev. Lett. **40**, 546 (1978).
[16] E. Jakeman, J. Phys. A **13**, 31 (1980).
[17] P. W. Anderson, Phys. Rev. **109**, 1492 (1958).
[18] C. P. Lapointe, P. Zakharov, F. Enderli, T. Feurer, S. E. Skipetrov, and F. Scheffold, Europhys. Lett. **105**, 34002 (2014).
[19] E. Abrahams, P. W. Anderson, D. C. Licciardello, and T. V. Ramakrishnan, Phys. Rev. Lett. **42**, 673 (1979).
[20] A. A. Chabanov, M. Stoytchev, and A. Z. Genack, Nature **404**, 850 (2000).
[21] S. Zhang, B. Hu, P. Sebbah, and A. Z. Genack, Phys. Rev. Lett. **99**, 063902 (2007).
[22] F. Riboli, P. Barthelemy, S. Vignolini, F. Intonti, A. De Rossi, S. Combrie, and D. S. Wiersma, Opt. Lett. **36**, 127 (2011).
[23] M. Stoytchev and A. Z. Genack, Phys. Rev. Lett. **79**, 309 (1997).
[24] H. Hu, A. Strybulevych, J. H. Page, S. E. Skipetrov, and B. A. van Tiggelen, Nat. Phys. **4**, 945 (2008).
[25] D. J. Thouless, Phys. Rev. Lett. **39**, 1167 (1977).
[26] S. A. van Langen, P. W. Brouwer, and C. W. J. Beenakker, Phys. Rev. E **53**, R1344 (1996).
[27] J. C. M. Garnett, Phil. Trans. R. Soc. A **205**, 237 (1906).
[28] P. Mallet, C. A. Guérin, and A. Sentenac, Phys. Rev. B **72**, 014205 (2005).
[29] J. B. Pendry, J. Phys. C **20**, 733 (1987).
[30] A. D. Stone, P. A. Mello, K. A. Muttalib, and J.-L. Pichard, in *Mesoscopic Phenomena in Solids*, edited by B. L. Altshuler, P. A. Lee, and R. A. Webb (North-Holland, Amsterdam, 1991).
[31] A. D. Mirlin, Phys. Rev. B **53**, 1186 (1996).
[32] P. Peier, H. Merbold, V. Pahinin, K. A. Nelson, and T. Feurer, New J. Phys. **12**, 013014 (2010).
[33] I. Reed, IRE Trans. Inf. Theory **8**, 194 (1962).
[34] S. Barkhofen, J. J. Metzger, R. Fleischmann, U. Kuhl, and H.-J. Stöckmann, Phys. Rev. Lett. **111**, 183902 (2013).
[35] H. Cao, Y. G. Zhao, S. T. Ho, E. W. Seelig, Q. H. Wang, and R. P. H. Chang, Phys. Rev. Lett. **82**, 2278 (1999).
[36] T. Hisch, M. Liertzer, D. Pogany, F. Mintert, and S. Rotter, Phys. Rev. Lett. **111**, 023902 (2013).